5-11-2016

The Primary Volatile Composition of Comet C/2012 K1 (PanSTARRS)

Nathaniel Xavier Roth
University of Missouri-St. Louis

The Primary Volatile Composition of Comet C/2012 K1 (PanSTARRS)

by

Nathaniel Xavier Roth

B.S. Physics, University of Missouri-St. Louis, 2014

A Thesis

Submitted to The Graduate School of the

University of Missouri-St. Louis

In partial fulfillment of the requirements of the degree

Master of Science

In

Physics

August 2016

Advisory Committee

Erika Gibb, Ph.D.

Chairperson

Bruce Wilking, Ph.D.

David Horne, Ph.D.

ABSTRACT

On 2014 May 22 and 24 we characterized the volatile composition of the dynamically new Oort cloud comet C/2012 K1 (PanSTARRS) using the long-slit, high resolution ($\lambda/\Delta\lambda \approx 25{,}000$) infrared echelle spectrograph (NIRSPEC) at the 10 m Keck 2 telescope on Maunakea, HI. We detected fluorescent emission from six primary volatiles (H_2O, HCN, CH_4, C_2H_6, CH_3OH, and CO). Upper limits were derived for C_2H_2, NH_3, and H_2CO. We report rotational temperatures, production rates, and mixing ratios (relative to water). Compared with median abundance ratios for primary volatiles in other sampled Oort cloud comets, trace gas abundance ratios in C/2012 K1 (PanSTARRS) for CO, CH_4, and HCN are consistent, but CH_3OH and C_2H_6 are enriched while H_2CO and possibly C_2H_2 are depleted. When placed in context with comets observed in the near infrared to date, the data suggest a continuous distribution of abundances of some organic volatiles among the comet population.

1. INTRODUCTION

Comets are among the most primitive remnants from the formation of the solar system. They were some of the first bodies to accrete in the solar nebula, forming in the outer (>5 AU) giant planet region. The chemical composition of their nuclei should reflect the chemical makeup of the midplane of the protoplanetary disk where (and when) they formed. Gravitational interactions with the giant planets during the final phases of planet formation ejected many comets into either the Oort cloud (Gladman 2005) or the Kuiper disk (scattered disk population, see Morbidelli & Brown 2004). These two regions make up the major dynamical reservoirs of the solar system for comets that become available for remote sensing using high-resolution spectroscopy.

Since their emplacement in the Oort cloud or the Kuiper disk, the interior compositions of cometary nuclei have remained (at least to a large degree) unchanged. Most processes considered to alter the properties of the nucleus during its (~4.5 billion years) residence in the Oort cloud (or the Kuiper disk) are expected to affect a thin (a few meters deep) layer near the surface (see Stern 2003 for a detailed discussion of these processes for Oort cloud comets). This layer is lost during a typical passage through the inner solar system. Due to the scattering processes that placed comets in their present-day reservoirs, the Oort cloud and Kuiper disk contain comets that may represent widely varying formation regions in the solar nebula. Determining the native volatile (i.e., as contained as ice in the nucleus) composition can provide insights into these formation regions and also the formation pathways (Levison et al. 2010).

As comets enter the inner solar system, increasing radiation from the sun causes native ices to sublimate and release primary volatiles into the coma (a freely expanding atmosphere, or exosphere), a dust tail, and an ion tail. Near infrared spectroscopy of

fluorescent emission can be used to characterize the primary volatile composition of the coma, and by inference the nucleus. Early results led to characterization of (at least) three taxonomic classes: "organics-depleted", "organics-normal", or "organics-enriched" (Mumma & Charnley 2011), based on measured abundance ratios (also termed "mixing ratios") of their primary volatiles relative to H_2O (the most abundant ice in comets). However, the compositions of some comets do not fit into any of these proposed taxonomic classes, challenging and requiring expansion of this classification system (Bonev et al. 2008a; Radeva et al. 2013; Gibb et al. 2012).

To that end, we add the volatile composition of comet C/2012 K1 (PanSTARRS) to the body of work, with the hope of further establishing the taxonomic classification of primary volatiles among comets. In section 2 we discuss our observations and data analysis. In section 3 we present our results. In section 4, we provide a detailed discussion of our results in the context of the comet population.

2. OBSERVATIONS AND DATA REDUCTION

Comet C/2012 K1 (PanSTARRS) (hereafter K1) was a dynamically new Oort cloud comet on its first journey into the inner Solar System (Nakano 2013). K1 reached perihelion (1.05 AU) on 2014 August 27 and was closest to Earth (0.95 AU) on 2014 October 31. On 2014 May 22 and 24, we observed K1 with the high-resolution ($\lambda/\Delta\lambda \sim$ 25,000), near infrared, long-slit echelle spectrograph NIRSPEC at the 10 m W.M. Keck Observatory (McLean et al. 1998) to characterize its volatile composition. The observing log is shown in Table 1. We targeted nine primary volatiles (CO, H_2O, C_2H_2, C_2H_6, CH_4, H_2CO, CH_3OH, HCN, and NH_3) and two product volatiles (OH* and NH_2). Observations were performed with a 3 pixel (0.43″) wide slit, using a standard ABBA nod pattern, with

a 12″ beam separation along the 24″ long slit. Combining spectra of the nodded beams as A-B-B+A cancelled emissions from thermal background, instrumental biases, and "sky" emission (lines and continuum) to second order. The data were dark subtracted, flat fielded, cleaned of cosmic ray hits and high dark current pixels, and corrected for anamorphic optics. A detailed description of the flux calibration (using BS-5447) and reduction procedure can be found in Bonev (2005, Appendix B), Radeva et al. (2010), Villanueva et al. (2011a) and references therein.

Atmospheric spectra were synthesized using the Line-By-Line Spectral Transmittance Model optimized for Mauna Kea's atmospheric conditions (Clough et al. 2005; Villanueva et al. 2011b). These models were used to determine column burdens for absorbing species in the atmosphere and to assign wavelength scales to the extracted spectra. The atmospheric models were binned to the resolution of the comet spectrum and normalized to the comet's continuum level. The atmospheric models were then subtracted from each row of the cometary spectra; co-addition of multiple rows resulted in the residuals shown in Figures 2-3.

Production rates (Q, molecules s^{-1}) were determined using the Q-curve methodology (e.g., Bonev 2005; DiSanti et al. 2001, Gibb et al. 2012), which averages the emission intensity on either side of and equidistant from the nucleus, stepped in 0.6-arcsec intervals along the slit, resulting in a "symmetric" Q-curve. A spherically symmetric outflow velocity $v_{gas}=0.8R_h^{-0.5}$ km s^{-1} was assumed (Bonev, 2005). The symmetric Q-values increase with nucleocentric distance due primarily to seeing, until reaching a terminal value, referred to as the global production rate.

Growth factors, defined as GF = Q_{global}/Q_{NC}, where Q_{NC} is the nucleocentric production rate, were determined for both the gas and the dust when there was sufficient signal-to-noise. Only water and ethane had sufficient signal-to-noise to constrain the growth factor. Both molecules have similar spatial profiles (see Figure 1) and provide similar growth factors (see Table 2). Hence, those growth factors were applied to the remaining molecules to determine the production rates.

The *g*-factors used to generate synthetic fluorescent emission models in this study were adopted from quantum mechanical models for each molecule. These models include CH_4 (Gibb et al. 2003), C_2H_6 ν_7 (Villanueva et al. 2011a), H_2O (Villanueva et al. 2012a), CH_3OH (Villanueva et al. 2011b), HCN (Villanueva et al. 2011b), H_2CO (DiSanti et al. 2006), OH* (Bonev et al. 2006), C_2H_2, CO (Villanueva et al. 2011b), and NH_3 (Villanueva et al. 2011a).

3. RESULTS

We detected fluorescent emission from six primary volatiles (H_2O, HCN, CH_4, CH_3OH, C_2H_6, and CO). We report production rates for these, and upper limits for C_2H_2, NH_3, and H_2CO in K1. Synthetic models of fluorescent emission for each targeted species were compared to observed residual line intensities, correcting each line for the monochromatic atmospheric transmittance at its Doppler-shifted wavelength (according to the geocentric velocity of the comet). A Levenberg-Marquardt nonlinear minimization technique (Villanueva et al. 2008) was used to fit fluorescent emission from all species simultaneously in each echelle order, allowing for high-precision results, including in crowded spectral regions containing many spectral lines within a single instrumental resolution element. Rotational temperatures were determined using correlation and

excitation analyses as described in Bonev (2005, pp. 53-65), Bonev et al. (2008b), DiSanti et al. (2006), and Villanueva et al. (2008). Rotational temperatures were extracted for individual species, and the best constrained was that of H_2O, whose lines are intrinsically bright and for which a broad range of excitation energies was sampled in order 26 of our KL2 setting. On May 22, retrieved rotational temperatures were in satisfactory agreement; the rotational temperature derived for H_2O was applied to species for which rotational temperatures could not be well constrained. [In general, rotational temperatures agree for different primary species within a comet (see for example Gibb et al. 2012 and references therein; also see section 3.2.1 of DiSanti et al. 2016), supporting this approach.] However, the H_2O rotational temperature was poorly constrained on May 24, owing to poor SNR in orders with temperature-sensitive water lines. Therefore, the May 22 H_2O rotational temperature was adopted. Spectra and best-fit fluorescence models are shown in Figures 2-3. Best-fit rotational temperatures, growth factors, production rates, and mixing ratios for each date are given in Table 2.

4. Discussion

The matter of classifying comets according to their primary volatile composition has proven to be a complex undertaking. Extensive work at optical wavelengths has revealed that comets can be classified as "typical" or "carbon-chain depleted" based on their product species (e.g., A'Hearn et al. 1995; Cochran et al. 2012, and references therein). Additional work has been done using radio observations, where no clear taxonomic classes have been found (Crovisier et al. 2009; Mumma & Charnley 2011, and references therein). A similar endeavor began in the infrared with comets 1P/Halley (Mumma et al. 1986), C/1995 O1 (Hale-Bopp) (Dello Russo et al. 2000; Dello Russo et

al. 2001; DiSanti et al. 2001; Magee-Sauer et al. 1999), and C/1996 B2 (Hyakutake) (Mumma et al. 1996; Dello Russo et al. 2002; DiSanti et al. 2003; Magee-Sauer et al. 2002). The primary volatile composition of these comets suggested that they are chemically similar objects (Mumma et al. 2003). Subsequent observations of comets C/1999 S4 (LINEAR) (Mumma et al. 2001) and 73P/Schwassmann-Wachmann 3B (Villanueva et al. 2006) showed two comets that were highly depleted in virtually all trace primary volatiles relative to water, while at the other extreme comet C/2001 A2 (LINEAR) (Magee-Sauer et al. 2008) (and later C/2007 W1 Boattini) was enriched in the sampled trace primary volatiles. These results formed the basis for the aforementioned (Section 1) three-tiered taxonomy based on primary volatile abundance ratios (organics-enriched, organics-normal, organics-depleted; e.g. see Mumma & Charnley 2011 and references therein)

Recent work has suggested that the 3-fold classification scheme is incomplete and more complex. For example, the primary volatile composition of comets 8P/Tuttle, C/2007 N3 (Lulin) and 2P/Encke (Bonev et al. 2008a; Gibb et al. 2012; Radeva et al. 2013) show no systematic enrichment, depletion, or similarity to the mean. Among these three comets, CH_3OH may be seen as a "smoking gun" that shows comet primary volatile compositions are more complex than the current taxonomic system. All three comets had high CH_3OH abundances while being depleted in other molecules, such as C_2H_2. This suggests that the chemical diversity among comets is perhaps more complex than the simple organics-enriched, organics-normal, and organics-depleted framework. In this context, it should be noted that the taxonomy based on product species now suggests as many as seven distinct groupings (Schleicher and Bair 2014; Cochran et al. 2015).

However, both dust and gas can contribute product species, complicating the comparison with the emerging taxonomy based on primary species alone.

How does the primary volatile composition of comet K1 compare to other sampled Oort cloud comets? Using primary volatile abundances reported in Oort cloud comets using near infrared spectroscopy (in order to minimize uncertainties caused by different instruments/telescopes and wavelength regimes), we define a cometary median (see Table 3) for each primary volatile commonly studied in the infrared. Also shown in Table 3 are the mixing ratios of these species in K1 (given as a weighted average for molecules detected on both dates). From these it can be seen that CH_3OH (3.92%) and C_2H_6 (1.19%) are enriched, CO (3.55%), CH_4 (0.88%), and HCN (0.16%) are consistent with the cometary median, H_2CO (<0.25%) is depleted, and the 3σ upper limit for C_2H_2 (<0.19%) suggests it may also be depleted.

The next natural question is whether the distribution of primary volatiles among comets is more nearly continuous versus distinct. Figure 4 shows histograms of abundances relative to water for HCN, C_2H_6, CH_3OH, and CH_4, respectively. For each molecule, most comets have abundances close to the median, with some showing enrichment in certain molecules and depletion in others. Overall, the abundances of well-sampled primary volatiles, such as C_2H_6 and CH_3OH, suggest the emergence of a continuous distribution. The addition of K1 emphasizes this. Prior to this study, there was a lack of comets with C_2H_6 abundances between 0.87% and 1.70% (between "average" and "enriched"; Figure 4, panel [B]). K1 falls in this gap, suggesting that the gap resulted from the relatively small number of comets studied. This also suggests that the apparent gap for CH_3OH abundances between 0.20% and 1.0% (between "depleted" and

"average"; Figure 4, panel [C]) may be filled with additional comet observations. Examination of Figure 4 also shows that the level of enrichment or depletion in a given comet does not necessarily correlate across all molecules sampled. One comet may be enriched in CH_3OH and consistent with normal in HCN (K1) while another may be depleted in CH_3OH but not in HCN (73P/SW 3B), challenging attempts to assign definitive taxonomic classes.

There are several unanswered questions that need to be addressed before the distribution of volatile abundances in comets can be understood. First, what is the range of abundances for trace volatiles in comets? Are the currently proposed "taxonomic end-members" (C/2001 A2 on the "enriched" end and C/1999 S4 on the "depleted" end) truly representative of compositional extremes? On the low abundance end, we are limited by technology and the sensitivity of state-of-the-art techniques. On the upper end, we are limited by the relatively small number of comets measured to date with adequate signal-to-noise ratio. Of the ~10^{11} cometary nuclei that reside in the Oort cloud (Emel'Yanenko et al. 2007), we have measured primary volatile abundances for < 30 comets in the infrared. For some molecules, most specifically C_2H_2 and OCS, that number is much lower, due principally to lack of sensitivity (in the case of C_2H_2) and/or spectral coverage (in the case of OCS) in our "standard" NIRSPEC settings.

However, we expect both areas to be addressed with the availability of a powerful new cross-dispersed spectrograph (iSHELL) at the NASA-IRTF (Rayner et al. 2012). As the answers to these questions become clearer, we may also ask whether the distribution of primary volatile abundances in comets is a primordial effect preserved from cometary formation in the solar nebula, or if we are instead sampling heterogeneous nuclei, such as

the binary comet 67P/Churyumov-Gerasimenko (Rickman et al. 2015). Clearly, more studies of the primary volatile compositions of comets are needed to answer these complex questions.

Acknowledgements

The data presented in this study were obtained using the W.M. Keck Observatory, which is operated as a scientific partnership among the California Institute of Technology, the University of California, and the National Aeronautics and Space Administration. The Observatory was made possible by the generous financial support of the W.M. Keck Foundation. We recognize and acknowledge the very significant cultural role and reverence that the summit of Mauna Kea has always had within the indigenous Hawaiian community. This study was generously funded by the NASA Missouri Space Grant Consortium and NSF Planetary Astronomy Grant AST-1211362. NASA supported this work through its Planetary Astronomy (proposal 11-PAST11-0045) and Astrobiology Programs (awarded by the NASA Astrobiology Institute to the Goddard Center for Astrobiology under proposal 13-13NAI7-0032).

References

A'Hearn, M.F., Millis, Robert C., Schleicher, D.O., et al. 1995, Icarus, 118, 223

Bonev, B.P. 2005, PhD thesis, The University of Toledo, http://astrobiology.gsfc.nasa.gov/Bonev_thesis.pdf

Bonev, B.P., Mumma, M.J., DiSanti, M.A., et al. 2006, ApJ, 653, 774

Bonev, B.P., Mumma, M.J., Villanueva, G.L., et al. 2007, ApJ, 661, L97

Bonev, B.P., Mumma, M.J., Radeva, Y.L., et al. 2008a, ApJ, 680, L61

Bonev, B.P., Mumma, M.J., Kawakita, H., Kobayashi, H, & Villanueva, G.L., 2008b, Icarus, 196, 241

Bonev, B.P., Mumma, M.J., Gibb, E.L., et al. 2009, ApJ, 699, 1563

Clough, S.A., Shephard, M.W., Mlawer, E.J., et al. 2005, JQSRT, 91, 233

Cochran, A.L., Barker, E.S., & Gray, C.L. 2012, Icarus, 218, 144

Cochran, A.L., Levasseur-Regourd, A.-C., Cordiner, M., et al. 2015, SSRv, 197, 9

Crovisier, J., Biver, N., Bockelée-Morvan, D., et al. 2009, EM&P, 105, 267

Dello Russo, N., DiSanti, M.A., Mumma, M.J., Magee-Sauer, K., & Rettig, T.W. 1998, Icarus, 135, 377

Dello Russo, N., Mumma, M.J., DiSanti, M.A., et al. 2000, Icarus, 143, 324

Dello Russo, N., Mumma, M.J., DiSanti, M.A., et al. 2001, Icarus, 153, 162

Dello Russo, N., Mumma, M.J., DiSanti, M.A., et al. 2002, JGRE, 107, 5-1

Dello Russo, N., DiSanti, M.A., Magee-Sauer, K., et al. 2004, Icarus, 168, 186

Dello Russo, N., Mumma, M.J., DiSanti, M.A., et al. 2006, Icarus, 184, 255

Dello Russo, N. Vervack, R.J., Jr., Weaver, H.A., et al. 2007, Nature, 448, 172

DiSanti, M.A., Mumma, M.J., Dello Russo, N., & Magee-Sauer, K. 2001,

Icarus, 153, 361

DiSanti, M.A., Mumma, M.J., Dello Russo, N., et al. 2003, JGRE, 108, 15-1

DiSanti, M.A., Bonev, B.P., Magee-Sauer, K., et al. 2006, ApJ, 650, 470

DiSanti, M.A., Villanueva, G.L., Milam, S.N., et al. 2009, Icarus, 203, 589

DiSanti, M.A., Villanueva, G.L., Paganini, L., et al. 2014, Icarus, 228, 167

DiSanti, M.A., Bonev, B.P., Gibb, E.L., et al. 2016, ApJ, 820, 34

Emel'Yanenko, V.V., Asher, D.J., & Bailey, M.E. 2007, MNRAS, 381, 779

Gibb, E.L., Mumma, M.J., Dello Russo, N., DiSanti, M.A., & Magee-Sauer, K. 2003, Icarus, 165, 391

Gibb, E.L., Bonev, B.P., & Villanueva, G.L., et al. 2012, ApJ, 750, 102

Gladman, B. 2005, Sci, 307, 71

Levison, H.F., Duncan, M.J., Brasser, R., & Kaufmann, D. E. 2010, Sci, 329, 187

Magee-Sauer, K., Mumma, M.J., DiSanti, M.A., Dello Russo, N., & Rettig, T.W. 1999, Icarus, 142, 498

Magee-Sauer, K., Mumma, M.J., DiSanti, M.A., & Dello Russo, N. 2002, JGRE, 107, 6-1

Magee-Sauer, K., Mumma, M.J., DiSanti, M.A., et al. 2008, Icarus, 194, 347

McLean, I.S., Becklin, E.E., Bendiksen, O., et al. 1998, Proc. SPIE, 3354, 566

Morbidelli, A. & Brown, M.E. 2004, Comets II, ed. M.C. Festou, H.U. Keller, & H.A. Weaver (Tucson: Univ. Arizona Press), 175

Mumma, M.J., Weaver, H.A., Larson, H.P., et al. 1986, Sci, 232, 1523

Mumma, M.J., DiSanti, M.A., Dello Russo, N., et al. 1996, Sci, 272, 1310

Mumma, M.J., Dello Russo, N., DiSanti, M.A., et al. 2001, Sci, 292, 1334

Mumma, M.J., Dello Russo, N., DiSanti, M.A., et al. 2001, IAUC, 7578, 2

Mumma, M.J., DiSanti, M.A., Dello Russo, N., et al. 2003, AdSpR, 31, 2563

Mumma, M.J. & Charnley, S.B. 2011, ARA&A, 49, 471

Nakano, S. 2013. C/2012 K1 (PANSTARRS). Nakano Note NK 2588;
http://www.oaa.gr.jp/~oaacs/nk/nk2588.htm

Paganini, L., Mumma, M.J., Villanueva, G.L., et al. 2012, ApJ, 748, L13

Paganini, L., Blake, G.A., Villanueva, G.L., et al. 2013, IAUC, 9263, 3

Paganini, L, Mumma, M.J., Villanueva, G.L., et al. 2014a, ApJ, 791, 122

Paganini, L., DiSanti, M.A., Mumma, M.J., et al. 2014b, AJ, 147, 15

Radeva, Y., Mumma, M.J., Bonev, B.P., et al. 2010, Icarus, 206, 764

Radeva, Y., Mumma, M.J., Villanueva, G.L., et al. 2013, Icarus, 223, 298

Rayner, J., Bond, T., Bonnet, M., et al. 2012, SPIE, 8446, 84462C

Rickman, H., Marchi, S., A'Hearn, M.F., et al. 2015, A&A, 583, A44

Schleicher, D. & Bair, A. 2014, Asteroids, Comets, Meteors, Session 4-2-1, Paper #7

Stern, S.A. 2003, Nature, 424, 639

Villanueva, G.L, Bonev, B.P., Mumma, M.J., et al. 2006, ApJ, 650, L87

Villanueva, G.L., Mumma, M.J., Novak, R.E., & Hewagama, T. 2008, Icarus
195, 34

Villanueva, G.L., Mumma, M.J., & Magee-Sauer, K. 2011a, JGRE, 116, 08012

Villanueva, G.L., Mumma, M.J., DiSanti, M.A. et al. 2011b, Icarus, 216, 227

Villanueva, G.L., Mumma, M.J., Bonev, B.P., et al. 2012a, JQSRT, 113, 202

Villanueva, G.L., DiSanti, M.A., Mumma, M.J., & Xu, L.-H. 2012b, ApJ, 747, 37

Villanueva, G.L., Mumma, M.J., DiSanti, M.A., et al. 2012c, Icarus, 220, 291

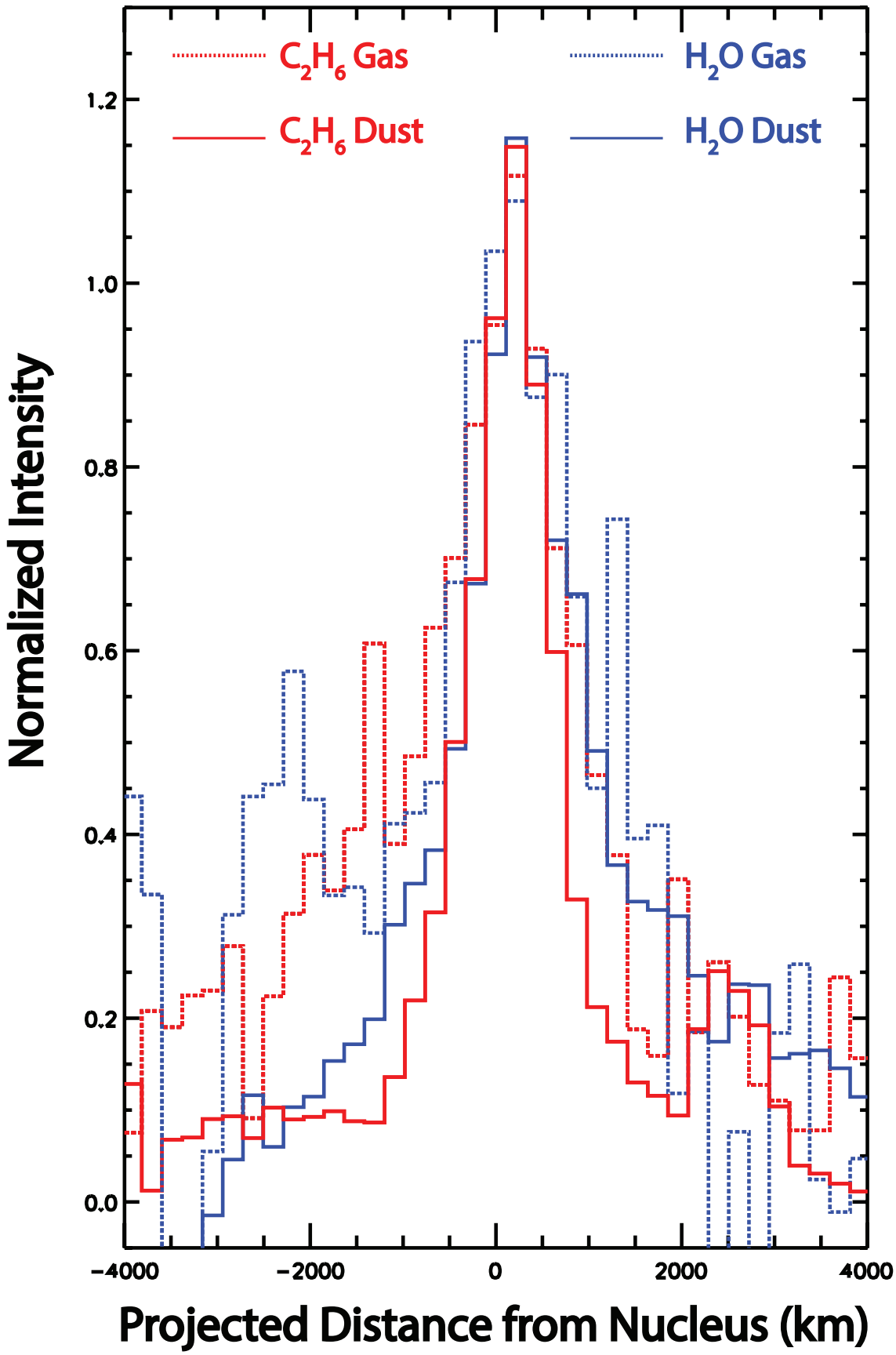
C_2H_6 Gas
C_2H_6 Dust
H_2O Gas
H_2O Dust
Normalized Intensity
0.0
0.2
0.4
0.6
0.8
1.0
1.2
−4000
−2000
0
2000
4000
Projected Distance from Nucleus (km)

Figure 1 – Emission spatial profiles of C_2H_6 gas (dashed red line), C_2H_6 dust (solid red line), H_2O gas (dashed blue line) and H_2O dust (solid blue line). All profiles are normalized to the mean intensity of the central three pixels.

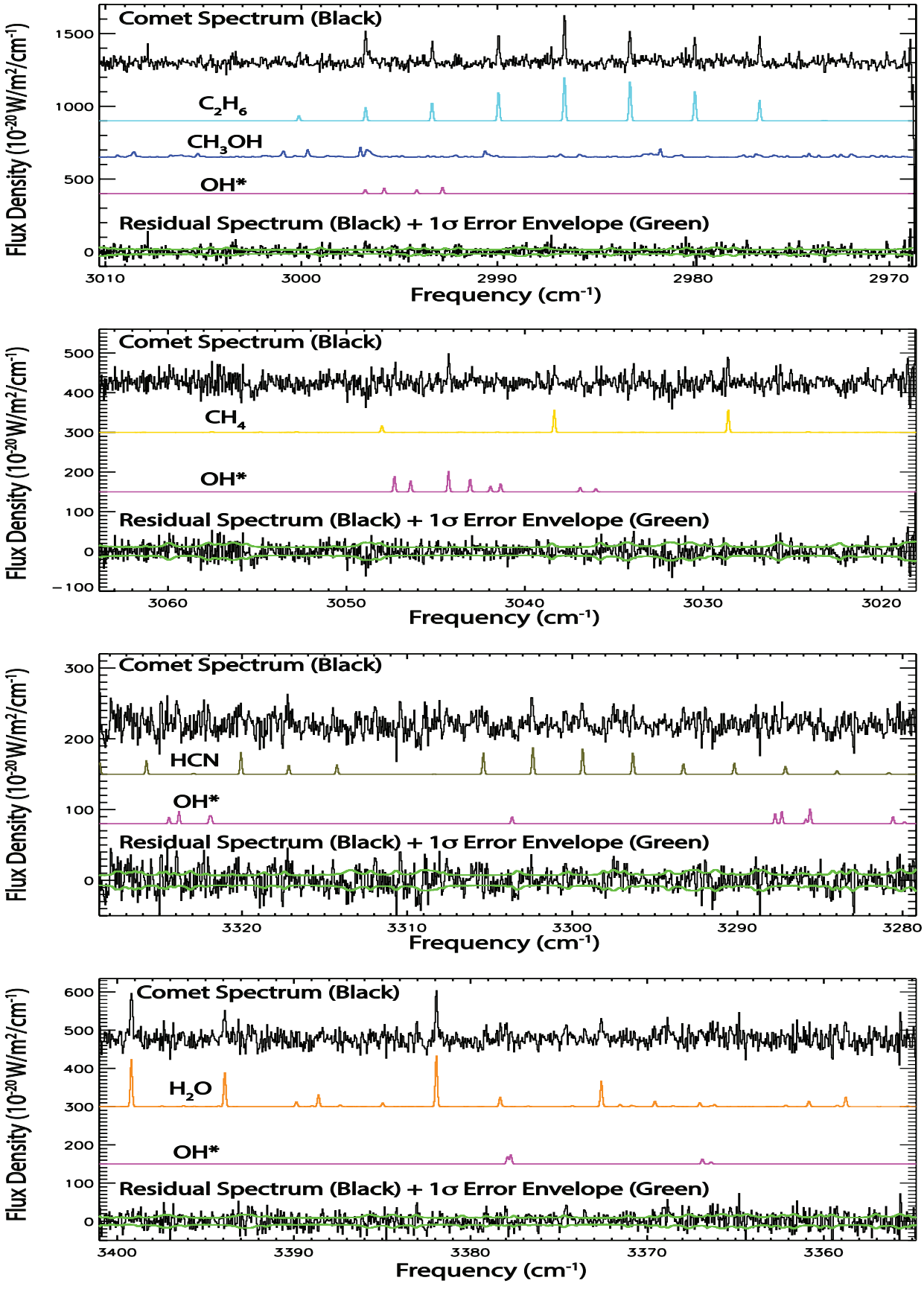
Comet Spectrum (Black)
C2H6
CH3OH
OH*
Residual Spectrum (Black) + 1σ Error Envelope (Green)
Flux Density (10-20W/m2/cm-1)
Frequency (cm-1)
Comet Spectrum (Black)
CH4
OH*
Residual Spectrum (Black) + 1σ Error Envelope (Green)
Flux Density (10-20W/m2/cm-1)
Frequency (cm-1)
Comet Spectrum (Black)
HCN
OH*
Residual Spectrum (Black) + 1σ Error Envelope (Green)
Flux Density (10-20W/m2/cm-1)
Frequency (cm-1)
Comet Spectrum (Black)
H2O
OH*
Residual Spectrum (Black) + 1σ Error Envelope (Green)
Flux Density (10-20W/m2/cm-1)
Frequency (cm-1)

Figure 2. Detections of C_2H_6, CH_3OH, H_2O, HCN, CH_4, and OH* in comet C/2012 K1 on 2014 May 22. The comet spectrum (after subtracting the telluric model) is plotted in black. Below are the individual best-fit fluorescent emission models contributing to that spectrum for OH* (purple), CH_3OH (blue), C_2H_6 (yellow), HCN (brown), CH_4 (gold), and H_2O (orange). The residual (spectrum – model, black) and 1σ error envelopes (green) are plotted at the bottom of each panel.

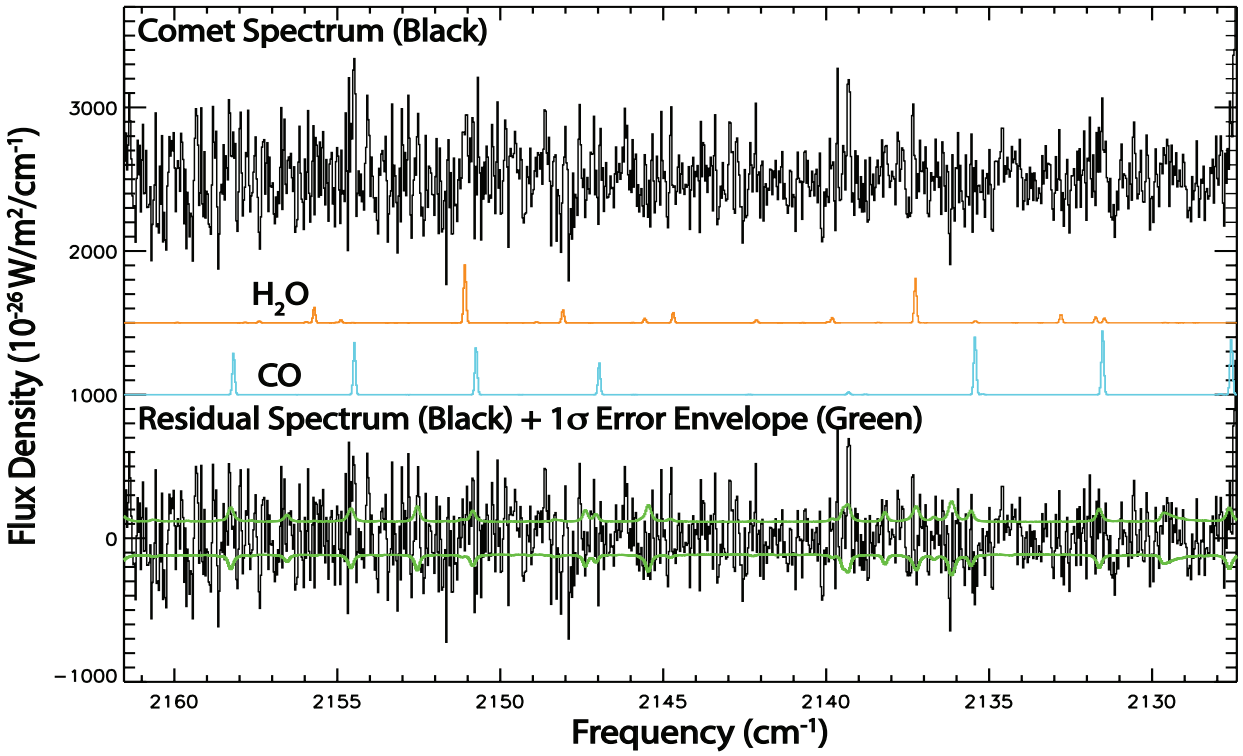

Figure 3. Detections of H_2O and CO on 2014 May 24. The comet spectrum (after subtracting the telluric model) is plotted in black. Below are the individual best-fit fluorescent emission models contributing to that spectrum for H_2O (orange) and CO (turquoise). The residual (model-spectrum, black) and 1σ error envelopes (green) are plotted at the bottom of the panel.

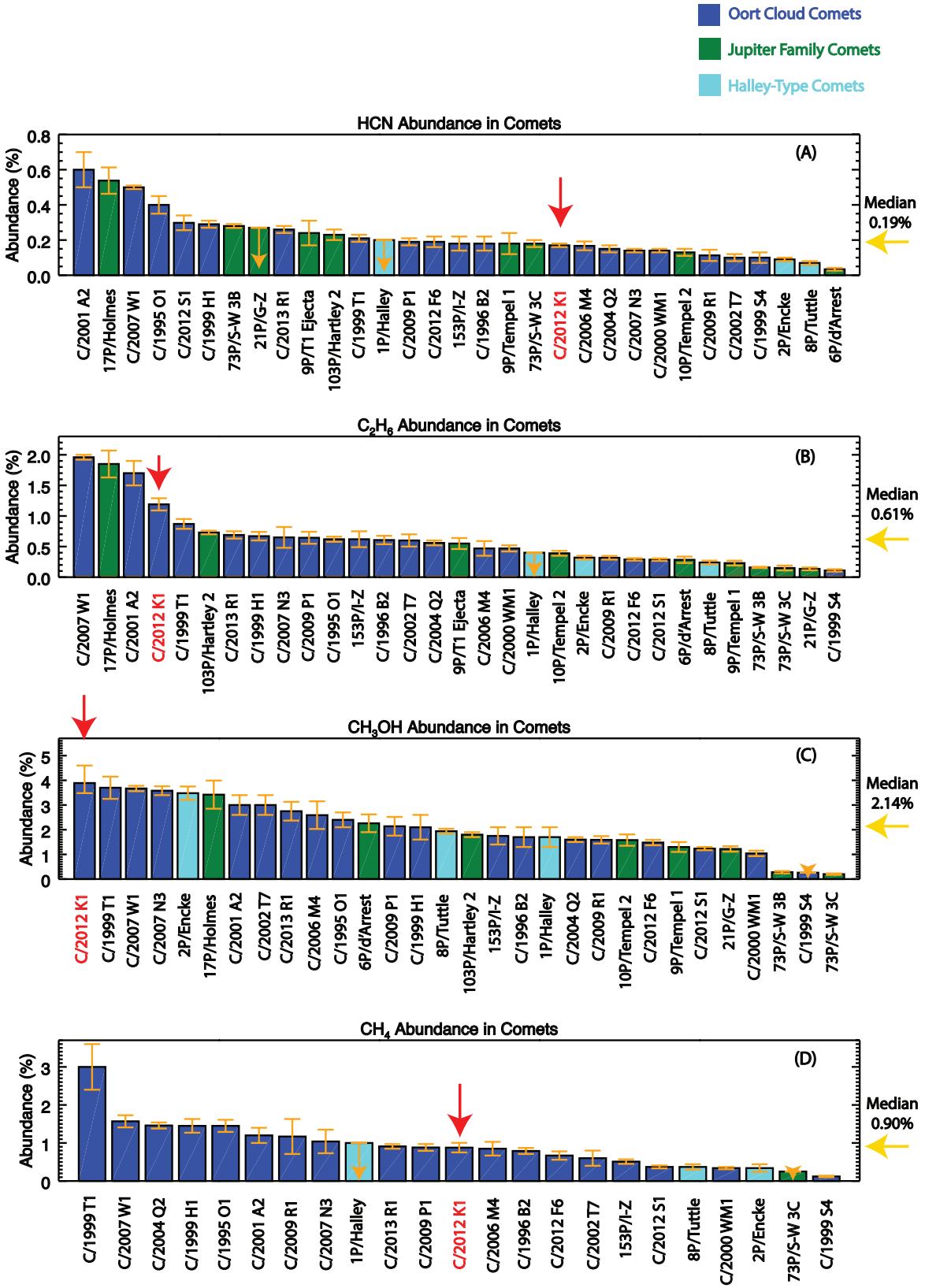
Oort Cloud Comets
Jupiter Family Comets
Halley-Type Comets
HCN Abundance in Comets
(A)
Abundance (%)
0.0
0.2
0.4
0.6
0.8
Median
0.19%
C/2001 A2
17P/Holmes
C/2007 W1
C/1995 O1
C/2012 S1
C/1999 H1
73P/S-W 3B
21P/G-Z
C/2013 R1
9P/T1 Ejecta
103P/Hartley 2
C/1999 T1
1P/Halley
C/2009 P1
C/2012 F6
153P/I-Z
C/1996 B2
9P/Tempel 1
73P/S-W 3C
C/2012 K1
C/2006 M4
C/2004 Q2
C/2007 N3
C/2000 WM1
10P/Tempel 2
C/2009 R1
C/2002 T7
C/1999 S4
2P/Encke
8P/Tuttle
6P/d'Arrest
C2H6 Abundance in Comets
(B)
Abundance (%)
0.0
0.5
1.0
1.5
2.0
Median
0.61%
C/2007 W1
17P/Holmes
C/2001 A2
C/2012 K1
C/1999 T1
103P/Hartley 2
C/2013 R1
C/1999 H1
C/2007 N3
C/2009 P1
C/1995 O1
153P/I-Z
C/1996 B2
C/2002 T7
C/2004 Q2
9P/T1 Ejecta
C/2006 M4
C/2000 WM1
1P/Halley
10P/Tempel 2
2P/Encke
C/2009 R1
C/2012 F6
C/2012 S1
6P/d'Arrest
8P/Tuttle
9P/Tempel 1
73P/S-W 3B
73P/S-W 3C
21P/G-Z
C/1999 S4
CH3OH Abundance in Comets
(C)
Abundance (%)
0
1
2
3
4
5
Median
2.14%
C/2012 K1
C/1999 T1
C/2007 W1
C/2007 N3
2P/Encke
17P/Holmes
C/2001 A2
C/2002 T7
C/2013 R1
C/2006 M4
C/1995 O1
6P/d'Arrest
C/2009 P1
C/1999 H1
8P/Tuttle
103P/Hartley 2
153P/I-Z
C/1996 B2
1P/Halley
C/2004 Q2
C/2009 R1
10P/Tempel 2
C/2012 F6
9P/Tempel 1
C/2012 S1
21P/G-Z
C/2000 WM1
73P/S-W 3B
C/1999 S4
73P/S-W 3C
CH4 Abundance in Comets
(D)
Abundance (%)
0
1
2
3
Median
0.90%
C/1999 T1
C/2007 W1
C/2004 Q2
C/1999 H1
C/1995 O1
C/2001 A2
C/2009 R1
C/2007 N3
1P/Halley
C/2013 R1
C/2009 P1
C/2012 K1
C/2006 M4
C/1996 B2
C/2012 F6
C/2002 T7
153P/I-Z
C/2012 S1
8P/Tuttle
C/2000 WM1
2P/Encke
73P/S-W 3C
C/1999 S4

Figure 4 – Abundances of HCN (panel A), C_2H_6 (panel B), CH_3OH (panel C), and CH_4 (panel D) in comets. Blue bars represent Oort cloud comets, green bars represent Jupiter Family comets, mint bars represent Halley-type comets, downward orange arrows represent 3σ upper limits, and the golden arrows on the right hand side show the median abundance for each molecule. K1 is highlighted with a red arrow illustrating how it fills in a gap between "average" and "enriched" comets in C_2H_6.

Table 1

Observing Log and H_2O Production Rates

UT Date	NIRSPEC Setting	UT	R_h (AU)	dR_h/dt (km s^{-1})	Δ (AU)	$d\Delta/dt$ (km s^{-1})	T_{int} (minutes)	$Q(H_2O)$ (10^{28} s^{-1})
2014 May 22	KL1	6:20-7:10	1.857	-20.32	1.556	14.94	43	4.02(0.27)
	KL2	7:18-8:46	1.857	-20.32	1.557	15.04	52	4.53(0.28)
2014 May 24	KL1	5:48-6:29	1.846	-20.30	1.565	15.44	27	4.83(0.27)
	MWA	6:39-8:37	1.845	-20.30	1.565	15.53	15	4.07(0.96)
	KL2	8:49-9:06	1.844	-20.29	1.566	15.73	19	5.41(0.79)

Notes. R_h, dR_h/dt, Δ, and $d\Delta/dt$ are heliocentric distance, heliocentric velocity, geocentric distance, and topocentric line-of-sight velocity, respectively, of C/2012 K1; T_{int} is total integration time on source, and $Q(H_2O)$ is the water production rate.

Table 2

Volatile Composition of Comet C/2012 K1 (PanSTARRS)

NIRSPEC Setting	Molecule	T_{rot}[a] (K)	Growth Factor[b]	Q[c,d] (10^{26} mol s^{-1})	Mixing Ratio[d] (%)
2014 May 22, R_h = 1.857 AU, Δ = 1.557 AU					
KL2	H_2O	44^{+5}_{-6}	1.7 ± 0.2[e]	453 ± 28	100
	H_2CO	(44)	(1.7)	< 1.11	< 0.25
	CH_4	(44)	(1.7)	3.97 ± 0.51	0.88 ± 0.13
	HCN	(44)	(1.7)	0.77 ± 0.11	0.17 ± 0.03
	C_2H_2	(44)	(1.7)	< 0.85	< 0.19
	NH_3	(44)	(1.7)	< 13.7	< 3.02
KL1	H_2O	(44)	1.7 ± 0.1[e]	402 ± 30	100
			2.3 ± 0.5[f]		
	C_2H_6	(44)	1.0 ± 0.3[e]	5.25 ± 0.46	1.31 ± 0.15
			2.0 ±0.1[f]		
	CH_3OH	(44)	(2.0)	15.5 ± 1.5[g]	3.84 ± 0.47
				19.2 ± 2.8[h]	4.78 ± 0.78
				16.3 ± 1.3[i]	4.10 ± 0.10
2014 May 24, R_h = 1.834 AU, Δ = 1.574 AU					
KL2	H_2O	(44)	2.0 ± 0.2[e]	407 ± 96	100
	HCN	(44)	(2.0)	0.64 ± 0.09	0.16 ± 0.04
KL1	H_2O	(44)	1.3 ± 0.2[e]	483 ± 27	100

			1.6 ± 0.2[f]		
	C_2H_6	(44)	(2.0)	5.34 ± 0.59	1.11 ± 0.14
	CH_3OH	(44)	(2.0)	15.5 ± 3.8	3.21 ± 0.82
	CH_4	(44)	(2.0)	< 4.37	< 0.91
MWA	H_2O	(44)	(2.0)	541 ± 79	100
	CO	(44)	(2.0)	19.2 ± 2.7	3.55 ± 0.72

Notes.

[a] Rotational temperature. Values in parentheses are assumed.

[b] Growth factor. Values in parentheses are assumed.

[c] Errors in production rate include line-by-line deviation between modeled and observed intensities and photon noise (see Bonev, 2005; Dello Russo et al. 2004; Bonev et al. 2007).

[d] Upper limits are 3σ

[e] Dust growth factor

[f] Gas growth factor

[g] CH_3OH production rate from KL1 Order 22

[h] CH_3OH production rate from KL1 Order 23

[i] Weighted average CH_3OH production rate from KL1 Order 22 and KL1 Order 23

Table 3

Abundance of Primary Volatiles in C/2012 K1 and Median in Oort Cloud Comets

Molecule	Abundance in K1[a]	Median Abundance in OC Comets[b]
C_2H_6	1.19%	0.61%
CH_3OH	3.92%	2.14%
CH_4	0.88%	0.90%
HCN	0.16%	0.19%
NH_3	< 3.02%	0.66%
C_2H_2	< 0.19%	0.17%
H_2CO	< 0.25%	0.38%
CO	3.55%	3.73%

Notes.

[a] Abundances are given as weighted averages for molecules detected on both dates.

[b] Cometary median calculated from primary volatile abundances in OC comets C/2007 W1 (Boattini) (Villanueva et al. 2011b), C/2001 A2 (LINEAR) (Magee-Sauer et al. 2008), C/2013 R1 (Lovejoy) (Paganini et al. 2014a), C/1999 H1 (Lee) (Dello Russo et al. 2006), C/1999 T1 (McNaught-Hartley) (Mumma et al. 2001), C/2007 N3 (Lulin) (Gibb et al. 2012), C/2009 P1 (Garradd) (Villanueva et al. 2012c; Paganini et al. 2012; DiSanti et al. 2014), C/1995 O1 (Hale-Bopp) (Dello Russo et al. 2000; Dello Russo et al. 2001; DiSanti et al. 2001; Magee-Sauer et al. 1999), 153P/Ikeya-Zhang (Dello Russo et al. 2004), C/1996 B2 (Hyakutake) (Dello Russo et al. 2002; DiSanti et al. 2003; Magee-Sauer et al. 2002), C/2002 T7 (LINEAR) (DiSanti et al. 2006), C/2004 Q2 (Machholz) (Bonev et al. 2009), C/2006 M4 (SWAN) (DiSanti et al. 2009), C/2000 WM1 (LINEAR)

(Radeva et al. 2010), C/2009 R1 (McNaught) (Milam et al., in preparation), C/2012 F6 (Lemmon) (Paganini et al. 2014b), C/2012 S1 (ISON) (Paganini et al. 2013; DiSanti et al., in press), and C/1999 S4 (LINEAR) (Mumma et al. 2001).